

DOI: 10.1002/cplu.201402279

Synthesis of NiGa₂O₄ Octahedron Nanocrystal with Exposed {111} Facets and Enhanced Efficiency of Photocatalytic Water Splitting

Shi-Xiong Zhou,^[a, b] Xiao-Jun Lv,^{*[a]} Chen Zhang,^[b] Xing Huang,^[a] Lei Kang,^[c] Zhe-shuai Lin,^[c] Yong Chen,^[a] and Wen-Fu Fu^{*[a, b]}

For the first time, octahedral NiGa₂O₄ nanocrystals having reactive pH-dependent {111} facets are synthesized through a facile hydrothermal route without using any template or organic surfactant. The {111} facets of octahedral NiGa₂O₄ display clearly enhanced photocatalytic generation of hydrogen and oxygen from water splitting and good photocatalytic stability. Density functional calculations suggest that mixed statistically occupied Ga/Ni (fourfold- and sixfold-coordinated Ga/Ni) are most likely to be exposed at the (111) surface of NiGa₂O₄, which is very favorable for enhancing the photocatalytic activities, and the photoelectrochemical properties show that the NiGa₂O₄ octahedron displays a better photocurrent than NiGa₂O₄ nanorods with the [100] growth direction. The transient photocur-

rent decay scan results demonstrate that the NiGa₂O₄ octahedron exposed {111} facet electrode exhibits a transient decay time of 4 s, whereas this time is only 2 s for NiGa₂O₄ nanorod electrodes with the [100] growth direction. This longer transient decay time indicates that the charge-carrier recombination rate is lower in the NiGa₂O₄ octahedron electrode, which will contribute to the enhancement of the photocatalytic activity. The present study also demonstrates that designing nanostructures with the appropriate morphology and surface structures is a feasible approach for enhancing the photoexcited charge-transfer lifetime and developing highly active semiconductor photocatalysts.

Introduction

Semiconductors have attracted great attention over the past few decades owing to their suitable physical and photochemical properties for the photocatalytic splitting of water.^[1] The structure and morphology of specially exposed high-reactivity facets of semiconductors nano- or microcrystals usually give them high photocatalytic activities owing to the particular surface atomic arrangements and unsaturated dangling bonds.^[2] As a typical example, the {111} facet of semiconductors has been demonstrated to possess a superior surface atomic structure and electronic band structure, which contribute significantly to the enhanced photocatalytic activity. Ye^[3] and co-workers have successfully prepared {111}-facet-exposed anatase TiO₂ single crystals by using both F⁻ and ammonia as the

capping reagents, and the {111} facet exhibits a much higher photocatalytic activity than the TiO₂ sample with dominant {010}, {101}, or {001} exposed facets. Guo^[4] et al. prepared three types of AgBr nanocrystals, evolved from cubes, through truncated cubes, and finally to high-symmetry octahedra, with an increased surface area ratio of {111} to {100}. More importantly, the as-prepared AgBr nanocrystals exhibited very clear facet-dependent catalytic properties, and the {111}-dominated octahedra showed the highest photocatalytic activities. However, owing to the rapid diminishing of highly reactive facets during the crystal growth process as a result of the minimization of surface energy, the synthesis of these highly reactive facets of nano- or microcrystals is still a difficult and challenging task.^[5]

Recently, gallate compounds have attracted attention in the areas of photocatalysis, adsorption, ion exchange, porous materials, and so on, owing to their high stability, high-energy laser systems, and high photocatalytic activities.^[6] NiGa₂O₄ crystallizes in the spinel structure, and is well known as a stable photocatalyst for photocatalytic hydrogen evolution from water. Hollow rods of nanocrystalline NiGa₂O₄ were prepared from Ga₂O₃ and Ni.^[7] However, the NiGa₂O₄ exposed high-reactivity facets showed a high photocatalytic hydrogen evolution activity that had not been reported previously. Furthermore, the development of template- and surfactant-free hydrothermal solution routes for the preparation of high-purity NiGa₂O₄ nanocrystals with controllable crystallographic facets still remains a great challenge.

[a] S.-X. Zhou, Dr. X.-J. Lv, Dr. X. Huang, Prof. Y. Chen, Prof. W.-F. Fu
Key Laboratory of Photochemical Conversion and Optoelectronic Materials
and HKU-CAS Joint Laboratory on New Materials
Technical Institute of Physics and Chemistry
Chinese Academy of Sciences, Beijing 100190 (P. R. China)
Fax: (+86) 10-82543520
E-mail: xjlv@mail.ipc.ac.cn
fuwf@mail.ipc.ac.cn

[b] S.-X. Zhou, C. Zhang, Prof. W.-F. Fu
College of Chemistry and Chemical Engineering
Yunnan Normal University, Kunming 650092 (P. R. China)

[c] L. Kang, Prof. Z.-s. Lin
Technical Institute of Physics and Chemistry
Chinese Academy of Sciences, Beijing 100190 (P. R. China)

 Supporting information for this article is available on the WWW under <http://dx.doi.org/10.1002/cplu.201402279>.

Here, for the first time, we synthesize the pH-dependent high-reactive {111} facets of octahedral NiGa₂O₄ nanocrystals through a facile hydrothermal route without using any template or organic surfactant, and the growth mechanism is investigated in detail. More importantly, in the absence of a cocatalyst, these {111} facets of octahedral NiGa₂O₄ display enhanced photocatalytic hydrogen and oxygen generation activities from water splitting and good photochemical stability, which has not been reported previously. In addition, we use first-principles calculations to study the surface structure and energy of the NiGa₂O₄ octahedrons, and the photoelectrochemical properties show that the NiGa₂O₄ octahedron displays a better photocurrent than NiGa₂O₄ nanorods with the [100] growth direction.

To the best of our knowledge, few investigations have focused on the effect of surfaces in different facet systems on photoexcited charge transfer as the fundamental process dominating chemical reactions and photoelectronic and photocatalytic processes,^[8] although a few reports have shown significant differences in electron transfer for different facet systems based on {101} and {001} of TiO₂.^[8,9] Herein, we use the transient photocurrent decay scan to demonstrate that the electrode of NiGa₂O₄ octahedrons with exposed {111} facets exhibits a transient decay time of 4 s, whereas this time is only 2 s for NiGa₂O₄ nanorod electrodes with the [100] growth direction. This longer transient decay time indicates that the charge-carrier recombination rate is lower in the NiGa₂O₄ octahedron electrode, contributing to the enhancement of its photocatalytic activity.

Results

Morphology and structure of octahedral NiGa₂O₄

The X-ray diffraction (XRD) pattern of octahedral NiGa₂O₄ in Figure 1a, shows that the diffraction peaks can be indexed

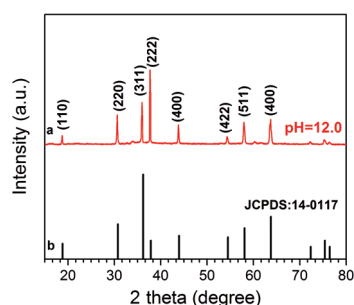


Figure 1. XRD patterns of as-prepared NiGa₂O₄ at pH 12.0.

easily to cubic NiGa₂O₄ with the spinel structure^[7] (JCPDS cards No.10-0114) with space group *Fd-3m* (227), and lattice constants of $a=b=c=8.269$ Å and $\alpha=\beta=\gamma=90^\circ$. Compared with the relative strength shown in the standard pattern (Figure 1b), the dominant (222) diffraction peak suggests that the as-synthesized products have a preferred orientation along the (111) planes, and the diffraction intensity ratio of (222)/(311) for

the NiGa₂O₄ octahedron is 1.24, which is enhanced significantly from the standard ratio of 0.21, revealing that these crystals are enclosed by eight well-defined {111} facets;^[4] this is further demonstrated below by high-resolution transmission electron microscopy (HRTEM) and selected-area electron diffraction (SAED).

The size and morphology of the as-prepared NiGa₂O₄ were characterized by scanning electron microscopy (SEM) and transmission electron microscopy (TEM) images. Figures 2A–C

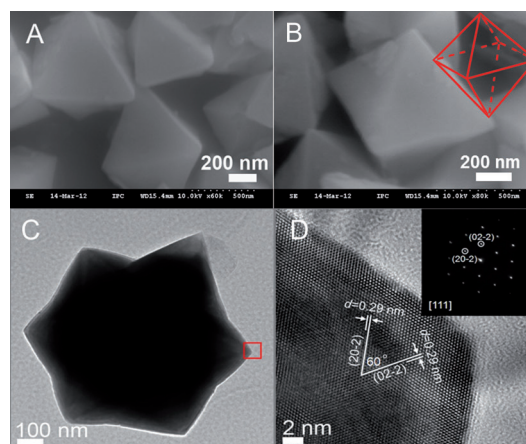


Figure 2. A) SEM image, B) enlarged SEM image, C) TEM, and D) HRTEM and SAED (inset) patterns of NiGa₂O₄ prepared at pH 12.0.

show that the as-synthesized NiGa₂O₄ consisted of a well-defined octahedral structure with {111} facets. Furthermore, on the basis of the analysis of the high-resolution TEM image (Figure 2D) taken from the red frame area indicated in Figure 2C, the interfacial angle between the (202) and (022) atomic planes (the same lattice spacing of 0.29 nm) of the NiGa₂O₄ octahedron is 60° , so we can confirm that the exposed crystal plane of NiGa₂O₄ is the {111} facet.^[3] The corresponding SAED pattern (inset in Figure 2D) confirms that the octahedron-shaped crystal is a single crystal, and the zone axis is indexed to be [111]. To the best of our knowledge, this is the first report on single-crystalline NiGa₂O₄ with exposed {111} facets. Energy-dispersive spectrum (EDS) analysis and X-ray photoelectron spectroscopy (XPS) confirmed the formation of the stoichiometric NiGa₂O₄ compound and displayed only the presence of Ga, Ni, and O elements (Figures S3, S4 in the Supporting Information). The UV/Vis absorbance spectrum of the NiGa₂O₄ octahedron was measured, and the bandgap was estimated to be 3.85 eV by extrapolating the linear region of a plot of the absorbance squared versus energy (Figure S5).

The pH value of the solution would clearly influence the structure and composition of NiGa₂O₄. With pH values in the range 4.0–10.0, the XRD and TEM results demonstrated that the precipitate was NiGa₂O₄ nanoparticles and that there was no octahedral NiGa₂O₄ with exposed {111} facets precipitated (Figure 3A–C). Figure 3D shows that the crystalline diffraction peaks became strong and narrow with increasing pH of the precursor solution, indicating the better crystallization of

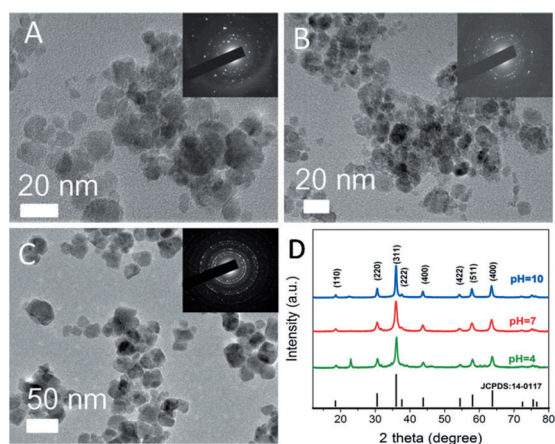


Figure 3. A–C) TEM images of the products obtained at pH values of 4.0, 7.0, and 10.0, respectively; D) corresponding XRD patterns of NiGa₂O₄ prepared at different pH values.

NiGa₂O₄. In addition, with the longer hydrothermal time of 36 h at pH 10, well-defined nanorods were obtained (Figure 4).

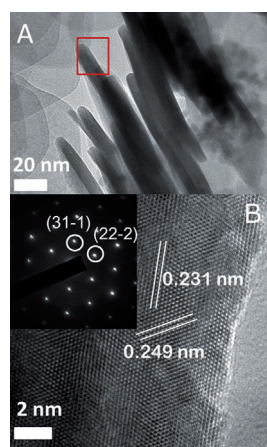


Figure 4. A) TEM image of NiGa₂O₄ nanorods. B) HRTEM image and SAED pattern taken from the white frame area indicated in Figure S10A. From the HRTEM image and the corresponding SAED pattern we can see that the nanorod is grown along the [100] direction.

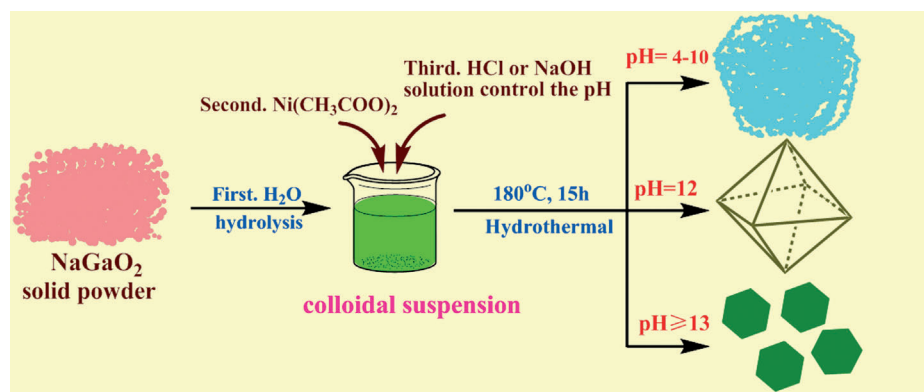
Table 1 and Figure S6 show that the surface area of synthesized NiGa₂O₄ changes significantly as the pH increases, which indicates that the OH⁻ concentration influences the process of cation exchange. Several research groups have discovered that kinetic control is very important for the nucleation and growth of nanocrystals.^[10] At pH 12.0, a well-defined NiGa₂O₄ octahedron was obtained. However, at pH ≥ 13, hexagonal sheet Ni(OH)₂ (JCPDS cards No. 14–0117) with the space group

Sample	pH value	Reaction temperature [°C]	Reaction time [h]	SBET [m ² g ⁻¹]
1	pH 4	180	15	49
2	pH 7	180	15	81
3	pH 10	180	15	46
4	pH 12	180	15	17

P-3m1 (164) was precipitated, with lattice constants of $a = b = 3.126 \text{ \AA}$, $c = 4.605 \text{ \AA}$, $\alpha = \beta = 90^\circ$, and $\gamma = 120^\circ$ (shown in Figure S7). The SEM image shows that the hexagonal Ni(OH)₂ has diameters of 100–400 nm, and the EDS pattern exhibits only Ni and O elements, with no Ga element (Figure S8). The reaction temperature and reaction time of the hydrothermal solution play an important role in the formation of the octahedral NiGa₂O₄ (Figures S9, S10). With increasing pH value, the number of free Ni²⁺ ions in the solution decreased because Ni²⁺ hydrolyzed into the hydrate, resulting in the slow nucleation of NiGa₂O₄ crystals.

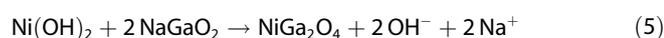
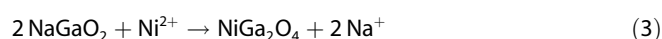
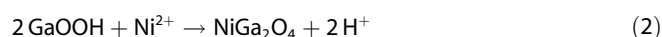
Formation mechanism of different crystals of NiGa₂O₄

A possible formation mechanism of different crystals of NiGa₂O₄ precipitated from precursor solutions of different pH in the hydrothermal process was supposed on the basis of observation of the effect of various experimental conditions and data in the literature (Scheme 1). The cations in the NaGaO₂ colloidal suspensions (for example, Na⁺ and H⁺) would first exchange with Ni²⁺ from the Ni(CH₃COO)₂ solution in the hydrothermal process.^[11] In an acidic environment (pH 4), the NaGaO₂ would react with H⁺ to form GaOOH, and the NiGa₂O₄ would be obtained through ion exchange of GaOOH and Ni²⁺ [Eqs. (1) and (2)].^[12] In a neutral environment (pH 7), the NaGaO₂ would also react with Ni²⁺ according to Equation (3) to form NiGa₂O₄.^[6b] In an alkaline environment (pH 10), the Ni²⁺ with the solution of the hydroxide reaction would generate nickel hydroxide, which would react with NaGaO₂ to form NiGa₂O₄ [Eqs. (4) and (5)].^[7] Kinetic control is very important for the nucleation and growth of the nanocrystals.^[10] If the nuclea-



Scheme 1. Growth mechanism for NiGa₂O₄ synthesized in solutions of different pH values.

tion becomes substantially slow, the nucleation and growth of the nanocrystals will be under kinetic control, and the final product can take a range of shapes that deviate from the thermodynamic ones.^[13] Therefore, the control of the nucleation kinetics was the key for the synthesis of octahedral NiGa₂O₄, and only if the conditions became favorable in a slow reaction process, would these highly anisotropic structures be formed. In general, at pH 12.0, the conditions are favorable to grow the NiGa₂O₄ octahedron.



Photocatalytic activity

The photocatalytic activities of different structures of NiGa₂O₄ were evaluated by monitoring the H₂ evolution from methanol aqueous solution under irradiation from a 300 W high-pressure mercury lamp. Considering the surface area effect on the photocatalytic activity, the Brunauer–Emmett–Teller (BET) specific surface areas were 49, 81, 46, and 17 m²g⁻¹ for the photocatalysts prepared at pH 4.0, 7.0, 10.0, and 12.0, respectively (see Table 1). We tested the photocatalytic performances of the different photocatalysts experimentally, without loading any cocatalyst,^[3] and the octahedral NiGa₂O₄ photocatalyst showed the highest photocatalytic hydrogen evolution activity; the H₂ evolution amount was 110 μmol after irradiation for 10 h without any cocatalyst, which is about four times that with a TiO₂ (P25) catalyst, three times that with NiGa₂O₄ nanoparticles at pH 7.0, 4.5 times that at pH 10.0, and six times that at pH 4.0 with NiGa₂O₄, demonstrating that the octahedral NiGa₂O₄ photocatalyst shows good photocatalytic activity and is promising for applications. In addition, the evolution of H₂ with different photocatalysts was also measured, and the normalized photocatalytic activities per surface area using 1% RuO₂-loaded NiGa₂O₄ (shown in Figure 5) show that the octahedral NiGa₂O₄ photocatalyst displays a higher photocatalytic hydrogen evolution activity than other photocatalysts.^[14]

The stability experiment results show that the hydrogen evolution amount of octahedral NiGa₂O₄ photocatalysts decreases only slightly after four photocatalysis cycles (40 h), and retains 95% of the initial activity (Figure 6). The XRD pattern confirmed the crystal structure of NiGa₂O₄ did not change after photocatalysis (Figure S11), indicating its good photocatalytic stability. The higher photocatalytic activity and stability of octahedral NiGa₂O₄ could be attributed to the hydrophilic ability, high surface energy of the {111} facet, and large percentages of undercoordinated metal (Ni and Ga) atoms on the surface of the {111} facet, which act as photocatalytic active sites in NiGa₂O₄.^[3,4] In addition, the different synthesis conditions (time and temperature) would affect not only the structure, but also

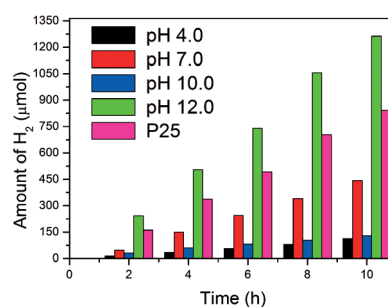


Figure 5. Normalized photocatalytic activities for the different photocatalysts (60 mg) using 1 wt% RuO₂-loaded NiGa₂O₄ and 1 wt% RuO₂-loaded P25 in methanol aqueous solution (30 mL) under UV/Vis light from a 300 W high-pressure Hg lamp.

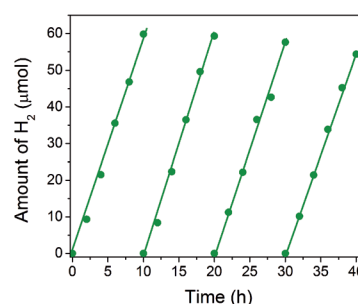


Figure 6. Hydrogen generation capability of different photocatalysts (60 mg) for H₂ evolution using methanol aqueous solution (30 mL) under UV/Vis light from a 300 W high-pressure Hg lamp.

the photocatalytic H₂ evolution activity of the NiGa₂O₄ nanocrystals.

For purposes of comparison, the NiGa₂O₄ nanorods were also used as photocatalysts under the same experimental conditions. The photocatalytic hydrogen evolution activity was also compared with that of the NiGa₂O₄ nanorods with the [100] growth direction prepared at pH 10.0 under hydrothermal conditions for 36 h (Figure 7). Interestingly, although the NiGa₂O₄ nanorods possess a specific surface area (51.5 m²g⁻¹) more than three times that (17 m²g⁻¹) of the octahedral NiGa₂O₄, their overall hydrogen evolution activity is lower than that of the latter; the amount of hydrogen (140 μmol h⁻¹) generated using the NiGa₂O₄ octahedrons as photocatalysts is clearly larger than that (78 μmol h⁻¹) generated using the NiGa₂O₄ nanorods with the [100] growth direction. The hydrogen production per surface area of the octahedrons is 137 μmol h⁻¹ m⁻², whereas that of the nanorods is only 25 μmol h⁻¹ m⁻², which suggests that the overall photocatalytic activity of the octahedrons is more directly related to its surface structure than to its specific surface area.

Control experiments were also performed in the absence of light irradiation or photocatalysts with magnetic stirring in the same quartz tube reaction vessel at room temperature, and no appreciable hydrogen or oxygen gas was detected for any system. This indicated that light irradiation was a prerequisite for the photocatalytic water splitting, and NiGa₂O₄ with 1 wt% RuO₂ photocatalyst can effectively split water to hydrogen under irradiation. The control experiments also demonstrated

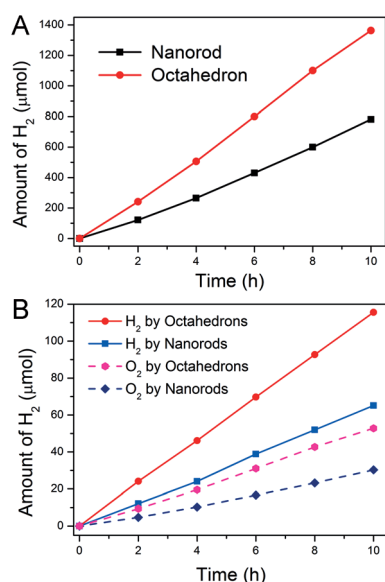


Figure 7. A) Photocatalytic hydrogen evolution from an aqueous methanol solution (30 mL, $V_{\text{H}_2\text{O}}:V_{\text{CH}_3\text{OH}} = 2:1$). B) Photocatalytic water splitting from pure water (30 mL) under UV/Vis light from a 300 W high-pressure Hg lamp over octahedron and nanorod NiGa_2O_4 photocatalysts (60 mg) with 1 wt% RuO_2 cocatalyst.

that the hydrogen and oxygen was generated through the photocatalytic reaction process, and not through the mechanocatalyst process.^[15]

Discussion

First-principles calculations study of the surface energy

To investigate further the facet effect on the photocatalytic properties of the NiGa_2O_4 material, we performed first-principles calculations to study the surface energy of the NiGa_2O_4 {111} facet. In this model, 14 atomic layers for the {111} surface were used. In particular, there are two kinds of statistical occupancies for Ga and Ni, that is, sixfold-coordinated Ga/Ni (54% Ga and 46% Ni) and fourfold-coordinated Ga/Ni (92% Ga and 8% Ni), corresponding to the brown and blue atom balls, respectively (Figure 8). There are three possible structures of the {111} surface of NiGa_2O_4 : a surface entirely constituted by O atoms; one consisting of sixfold-coordinated Ga/Ni; and one of mixed statistically occupied Ga/Ni (fourfold- and sixfold-coordinated Ga/Ni), that is, the 1st, 2nd, and 3rd surfaces displayed in Figures 8a, b, and c, respectively. The total energy calculation shows that the most stable mixed statistically occupied Ga/Ni atoms are most likely to be exposed at the {111} surface of NiGa_2O_4 (Figure 8c). Furthermore,

mixed statistical coordinations provide many more Ga/Ni atoms on the surface, and all the Ga/Ni atoms are coordinatively unsaturated; one is located in three-coordinated sites with three dangling bonds (corresponding to the brown sites), and the other is located in three-coordinated sites with one dangling bond (corresponding to the blue sites), which will provide more catalytically active sites to enhance the photocatalytic activity of NiGa_2O_4 .^[2d,3,4] To expand the visible light absorption, we have synthesized NiGa_2O_4 heterogeneously with stannous oxide, and showed robust H₂ evolution during visible light irradiation; a detailed study is under way.

Photoelectrochemical methods to study the different charge transfer for {111} and {001} facets

The photoelectrochemical (photocurrent–voltage) properties of the electrodes (of the NiGa_2O_4 octahedra and nanorods with [100] growth direction) show that an enhanced photocurrent is obtained over the entire potential range for the NiGa_2O_4 octahedra (Figure 9). Figure 9a displays the linear sweep voltammograms (at a scan rate of 20 mV s^{-1}) in the dark and under illumination for the NiGa_2O_4 octahedra and nanorod electrodes, respectively. The results show that the currents were almost

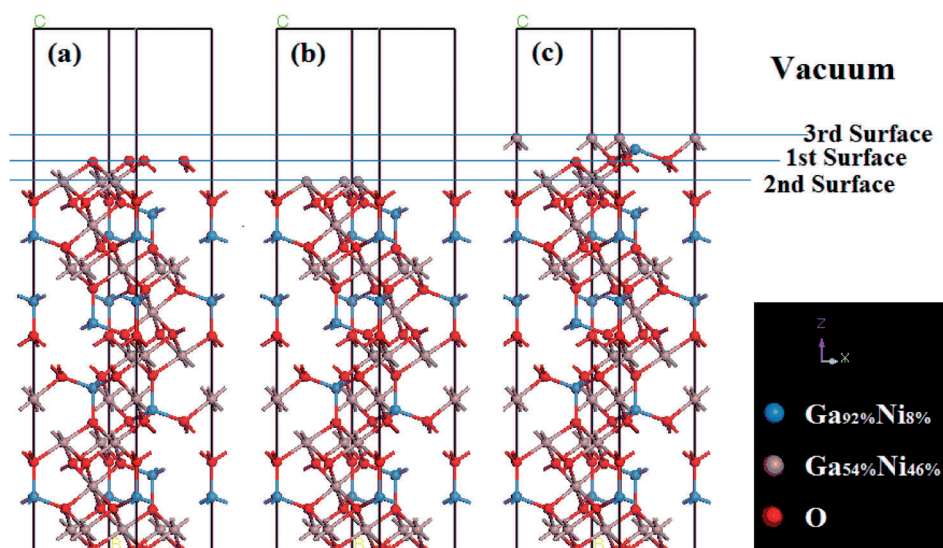


Figure 8. Relaxed geometries for the {111} surfaces with a) O atom surfaces, b) sixfold-coordinated Ga/Ni, and c) mixed fourfold- and sixfold-coordinated Ga/Ni based on a model of 14 atomic layers.

negligible in the dark, whereas the photocurrents increased steadily with applied positive potential under UV/Vis light illumination. The photocurrent density of the NiGa_2O_4 octahedron is more than twice the value for the nanorods over the entire potential range from 0.3 to 0.4 V. Clearly, the NiGa_2O_4 octahedron electrode shows a dramatically higher performance than the NiGa_2O_4 nanorod electrode. Figure 9b shows the linear sweep voltammograms of the NiGa_2O_4 octahedron and nanorod electrodes under chopped illumination, respectively. The NiGa_2O_4 octahedron electrode clearly exhibits a much more intense response than the NiGa_2O_4 nanorod electrode. These

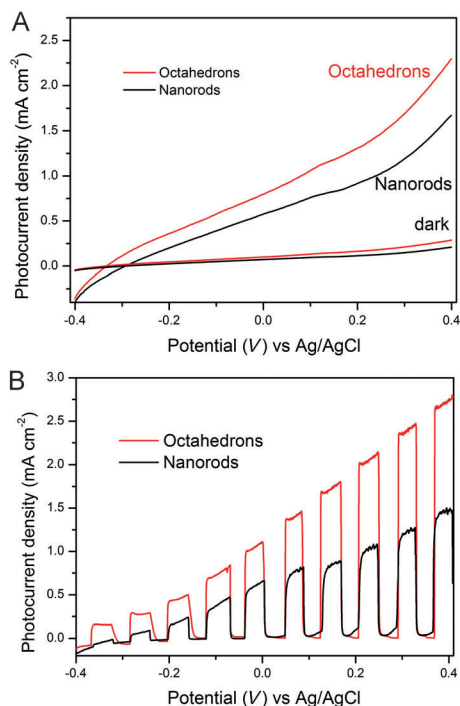


Figure 9. Linear sweep voltammograms of a) NiGa₂O₄ octahedra and nanorods. b) Potentiodynamic scans under chopped illumination for NiGa₂O₄ octahedra and nanorods under UV/Vis irradiation with a 300 W Xe lamp; in chopping mode, in 0.1 mol L⁻¹ NaClO₄ aqueous solution and 10% v/v methanol.

measurements demonstrate that the exposed {111} facet of the octahedron is more efficient than the nanorod with [100] growth direction in terms of photoenergy conversion.

Electron transport in NiGa₂O₄ octahedron and nanorod on the basis of photocurrent transient analyses

To further understand the superiority of NiGa₂O₄ octahedrons with exposed {111} facets over the nanorod electrodes with the [100] growth direction, we investigated the transient photocurrent decay observed immediately upon illumination to yield a qualitative understanding of the charge recombination behavior in the NiGa₂O₄ octahedrons and nanorod electrodes. Some researchers have investigated the charge recombination behavior through transient photocurrent decay measurements, for example, Amal et al. and our group have studied TiO₂/reduced graphene oxide composite electrodes,^[16] and Zhang et al. demonstrated the longer transient decay time for the Bi₂WO₆ 2D array.^[17] Figure 10A shows a schematic profile of a photocurrent transient response. Figure 10B shows the transient photocurrent scans obtained for the NiGa₂O₄ octahedrons with exposed {111} facets and the nanorod electrodes with the [100] growth direction under chopped illumination. Upon illumination of the electrode, we observe a relatively large photocurrent spike (I_{in}), which is attributed to the sudden photoinduced separation of electron–hole pairs. The spike then decays as the charge carriers are transported to the surface of the semiconductor and undergo the recombination process,^[16a,17] that is, the holes that reach the NiGa₂O₄ surface may accumu-

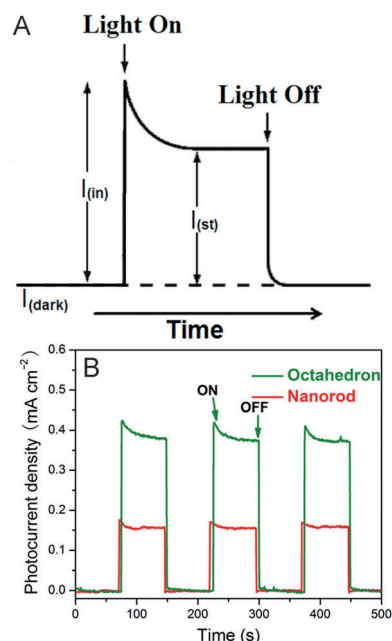


Figure 10. A) Schematic illumination of a photocurrent transient response curve. B) Photocurrent transient scans under chopped illumination over the NiGa₂O₄ octahedron electrode and nanorod electrode. Potential: 0 V applied bias versus Ag/AgCl.

late at the surface and recombine with the photogenerated electrons instead of capturing electrons from the electrolyte. In other words, the decay is determined by the rate at which minority carriers trapped in surface states capture majority carriers.^[17,18] Amal et al. proposed that the photocurrent decay rate is determined by the degree to which recombination dominates the charge generation process.^[15a] A steady-state current (I_{st}) is achieved as the charge generation and recombination rates reach equilibrium. Therefore, lower recombination rates should give rise to longer transient decay times.^[16a,17–19] The transient decay times τ of the NiGa₂O₄ octahedrons with exposed {111} facets and the nanorod electrodes with the [100] growth direction were calculated from a logarithmic plot of the parameter D according to Equation (6).

$$D = \frac{I_t - I_{st}}{I_{in} - I_{st}} \quad (6)$$

Here, I_t is the current at time t , I_{in} is the photocurrent spike, and I_{st} is the steady-state current (Figure 10A). The method allows a qualitative comparison of the electron lifetime within the films.^[16a,17,19] The transient decay time τ is defined as the time at which $\ln D = -1$.^[16a,17,19] The transient decay times of the NiGa₂O₄ octahedrons with exposed {111} facets and the nanorod electrodes with the [100] growth direction were thus calculated on the basis of the photocurrent profiles given in Figure 10B. The electrode of NiGa₂O₄ octahedrons with exposed {111} facets exhibits a transient decay time of 4 s, whereas the NiGa₂O₄ nanorod electrodes with the [100] growth direction give a time of only 2 s (Figure 11). This longer transient decay time indicates that the charge-carrier recombination rate

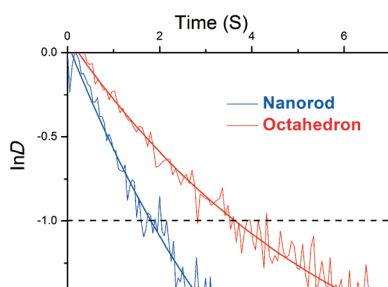


Figure 11. Plots of $\ln D$ as the transient decay time for the NiGa_2O_4 octahedra (red) and nanorod (blue) electrodes with no applied biases.

is lower in the NiGa_2O_4 octahedron electrode, contributing to the enhancement of the photocatalytic activity.

Conclusion

In conclusion, exposed {111} facets of octahedral NiGa_2O_4 were obtained through a facile hydrothermal synthesis for the first time; these nanocrystals displayed a remarkable enhancement of the photocatalytic water splitting for H_2 and O_2 evolution, showing that the octahedral NiGa_2O_4 photocatalyst has a good photocatalytic activity. Density functional theory results suggested mixed statistically occupied Ga/Ni atoms are most likely to be exposed at the (111) surface of NiGa_2O_4 ; these are very favorable for enhancing the photocatalytic activity. The photoelectrochemical properties showed that the NiGa_2O_4 octahedra displayed a better photocurrent than NiGa_2O_4 nanorods with the [100] growth direction. Few investigations have focused on the effect of surfaces in different facet systems on photoexcited charge transfer; here, we used the transient photocurrent decay scan to demonstrate that the electrode of NiGa_2O_4 octahedra with exposed {111} facets exhibits a transient decay time of 4 s, whereas this value is only 2 s for the NiGa_2O_4 nanorod electrode with the [100] growth direction. This longer transient decay time indicates that the charge-carrier recombination rate is lower in the NiGa_2O_4 octahedron electrode, contributing to its enhanced photocatalytic activity.

Experimental Section

Preparation of samples

All chemicals were of analytical purity and used as received without further purification. The NiGa_2O_4 catalysis samples were prepared through a modified ion-exchange method by modifying the work of Zou et al.^[6b] The NaGaO_2 pioneer (Figures S1, S2) was first prepared by calcining the mixture of Ga_2O_3 and Na_2CO_3 (molar ratio 1:1) at 700°C for 6 h; the resultant white solid was milled into a powder and heated at 900°C for a further 10 h. The NaGaO_2 colloidal suspension (0.2 mol L^{-1} , 10 mL) was added to an aqueous solution of $\text{Ni}(\text{CH}_3\text{COO})_2$ (0.05 mol L^{-1} , 20 mL) and stirred for 1 h at room temperature to form a homogeneous solution. The pH was adjusted from 4 to 13 by using HCl (1 mol L^{-1}) or NaOH (1 mol L^{-1}) solution, and stirring for 1 h. The obtained suspension solution was transferred into a Teflon-lined autoclave and treated thermally at 180°C for 15 h. The obtained precipitate was washed several times

with HCl (0.1 mol L^{-1}) and distilled water. The obtained precipitate was subsequently dried in an oven overnight at 70°C .

The 1 wt % RuO_2 -loaded NiGa_2O_4 was prepared through an impregnation method using $\text{Ru}_3(\text{CO})_{12}$ (Aldrich, 99%) as the starting material. The prepared NiGa_2O_4 was impregnated with $\text{Ru}_3(\text{CO})_{12}$ in THF, dried at 80°C , and oxidized in air at 500°C for 5 h to convert the loaded Ru complex into dispersed RuO_2 particles.

Characterizations

The crystal structure was determined with a Bruker D8 focus Powder X-ray diffractometer (XRD) with $\text{CuK}\alpha$ radiation ($\lambda = 1.5418\text{ \AA}$) in the 2θ range $10\text{--}80^\circ$. Transmission electron microscopy (TEM) images and selected-area electron diffraction (SAED) patterns were collected with a JEM-2100F (JEOL) microscope with an accelerating voltage of 200 kV. Scanning electron microscopy (SEM) was performed with a field-emission scanning electron microscope (Hitachi S-4300). UV/Vis diffuse reflectance spectra (DRS) were obtained on a Hitachi UV-3010 spectrophotometer using BaSO_4 as a reference. The Brunauer–Emmett–Teller (BET) surface areas were measured with a nitrogen physisorption Quadrasorb SI-MP surface area analyzer. The desorption isotherm was used to determine the pore size distribution by using the Barret–Joyner–Halender (BJH) method, assuming a cylindrical pore model. X-ray photoelectron spectroscopy (XPS) data were obtained with an ESCALab220i-XL electron spectrometer from VG Scientific using 300 W $\text{AlK}\alpha$ radiation. The base pressure was about 3.0×10^{-9} mbar. The binding energies were referenced to the C 1s line at 284.8 eV from adventitious carbon.

Photocatalytic activity evaluation

Hydrogen evolution was achieved in a 50 mL quartz tube containing photocatalysts in water and methanol solution (30 mL, v/v = 2:1). The quartz tube was sealed with a rubber septum and degassed by bubbling N_2 through the solution for 30 min at atmospheric pressure. Then, the mixture was irradiated with a 300 W high-pressure Hg lamp. All the experiments were conducted at room temperature with distilled water. The hydrogen generated from the systems was measured by gas chromatography (GC-14C, Shimadzu Co.); the chromatograph was equipped with a column (3 m \times 2 mm) of 5 \AA molecular sieves, a thermal conductivity detector, and nitrogen carrier gas. The hydrogen evolution was calculated versus the external standard method. The cycle stability of photocatalysts was determined by opening the sealed cuvette to release the hydrogen after every cycle, and degassing again by bubbling N_2 through the solution for 40 min, then sealing the cuvette with a rubber septum for the next photocatalytic reaction.

Photoelectrochemical experiments

The film electrodes of NiGa_2O_4 for the photoelectrochemical response measurements were fabricated first. The powders and ethanol containing Nafion solution (20 μL , 2 wt%) were mixed homogeneously (150 mg mL^{-1}), and the obtained paste was then spread on the conducting fluorine-doped SnO_2 glass substrate (FTO, 15 Ω /square) with a glass rod, using adhesive tapes as spacers. Finally, the resultant films had a thickness of about 4 μm thickness and active area of 1 cm^2 .

Photocurrent–voltage results were measured in a three-electrode configuration; the different morphologies of NiGa_2O_4 photoanodes

served as the working electrodes with an active area of about 1 cm², platinum was used as the counter electrode, and Ag/AgCl was used as the reference electrode; a 300 W Xe lamp was used as the illumination light source. The electrolyte was 0.1 M NaClO₄ and 10 vol% methanol solution, and this was purged continuously with N₂ for 20 min before the measurements. The photocurrents were recorded on a Chenhua electrochemical workstation.

Photocurrent transient response spectra under chopped illumination were measured in a two-electrode configuration, in which the NiGa₂O₄ photoanodes served as the working electrodes with an active area of about 1 cm² and a platinum wire was used as the counter electrode. The generated photocurrent signals were collected on a Chenhua electrochemical workstation. A 300 W Xe lamp was used as the light source. The electrolyte was 0.1 M KNO₃ aqueous solution.

Computational methods

The first-principles calculations for the NiGa₂O₄ {111} facet were performed through the plane-wave pseudopotential method^[20] implemented in the CASTEP package^[21] on the basis of density functional theory (DFT).^[22] The ion-electron interactions were modeled by the optimized normal-conserving pseudopotentials^[23] for all constituent elements, and the O 2s²2p⁴, Ni 3d⁸4s², and Ga 3d¹⁰4s²4p¹ electrons were treated as the valence electrons. The local density approximation (LDA)^[24] with a high kinetic energy cutoff of 750 eV and medium Monkhorst-Pack *k*-point meshes^[25] with a spanning of less than 0.05 Å³ in the Brillouin zone was adopted for the calculations. The virtual crystal approximation (VCA)^[26] was adopted to take into account the weight average of the potential of each atomic species, because the occupancies for all Ga and Ni atoms were distributed statistically in the NiGa₂O₄ crystal. Our tests revealed that the above computational setups were sufficiently accurate for the present purposes.

Acknowledgements

This study was financially supported by the National Key Basic Research Program of China (973 Program 2013CB834804, 2013CB632403) and the Ministry of Science and Technology (2012DFH40090). We thank the Natural Science Foundation of China (21107117, 21273257, 21353002, 21477136) and the Beijing Natural Science Foundation (2132057) for financial support.

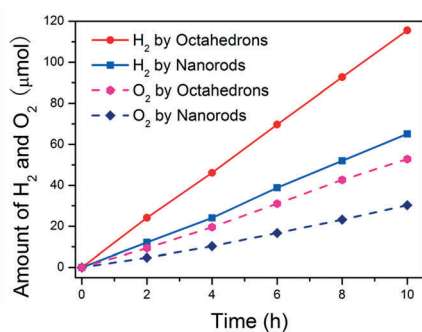
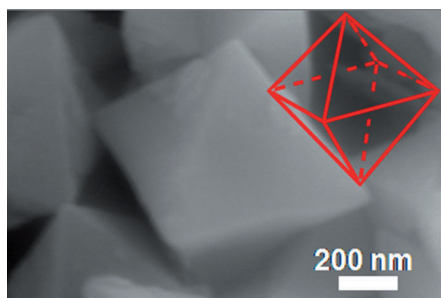
Keywords: density functional calculations · hydrothermal synthesis · octahedral NiGa₂O₄ · photocatalytic activity · water splitting

- [1] a) Z. Zou, J. Ye, K. Sayama, H. Arakawa, *Nature* **2001**, *414*, 625–627; b) P. D. Tran, L. H. Wong, J. Barber, J. S. C. Loo, *Energy Environ. Sci.* **2012**, *5*, 5902–5918; c) H. Zhou, Y. Qu, T. Zeid, X. Duan, *Energy Environ. Sci.* **2012**, *5*, 6732–6743; d) A. Kubacka, M. Fernández-García, G. Colón, *Chem. Rev.* **2012**, *112*, 1555–1614; e) X. Wang, Q. Xu, M. Li, S. Shen, X. Wang, Y. Wang, Z. Feng, J. Shi, H. Han, C. Li, *Angew. Chem. Int. Ed.* **2012**, *51*, 13089–13092; *Angew. Chem.* **2012**, *124*, 13266–13269; f) T. Ohno, L. Bai, T. Hisatomi, K. Maeda, K. Domen, *J. Am. Chem. Soc.* **2012**, *134*, 8254–8259; g) I. Tsuji, H. Kato, A. Kudo, *Angew. Chem. Int. Ed.* **2005**, *44*, 3565–3568; *Angew. Chem.* **2005**, *117*, 3631–3634; h) M. Kitano, M. Hara, *J. Mater. Chem.* **2010**, *20*, 627–641; i) X. J. Lv, W. F. Fu, H. X. Chang,

- H. Zhang, J. S. Cheng, G. J. Zhang, Y. Song, C. Y. Hu, J. H. Li, *J. Mater. Chem.* **2012**, *22*, 1539–1546.
- [2] a) H. Lin, L. Li, M. Zhao, X. Huang, X. Chen, G. Li, R. Yu, *J. Am. Chem. Soc.* **2012**, *134*, 8328–8331; b) H. G. Yang, C. H. Sun, S. Z. Qiao, J. Zou, G. Liu, S. C. Smith, H. M. Cheng, G. Q. Lu, *Nature* **2008**, *453*, 638–641; c) J. Pan, G. Liu, G. Q. M. Lu, H.-M. Cheng, *Angew. Chem. Int. Ed.* **2011**, *50*, 2133–2137; *Angew. Chem.* **2011**, *123*, 2181–2185; d) H. Tong, S. Ouyang, Y. Bi, N. Umezawa, M. Oshikiri, J. Ye, *Adv. Mater.* **2012**, *24*, 229–251; e) M. Sun, S. Xiong, X. Wu, C. He, T. Li, P. K. Chu, *Adv. Mater.* **2013**, *25*, 2035–2039; f) P. A. Morris Hotsenpiller, J. D. Bolt, W. E. Farneth, J. B. Lowekamp, G. S. Rohrer, *J. Phys. Chem. B* **1998**, *102*, 3216–3226; g) T. Ohno, K. Sarukawa, M. Matsumura, *New J. Chem.* **2002**, *26*, 1167–1170.
- [3] H. Xu, P. Reunchan, S. Ouyang, H. Tong, N. Umezawa, T. Kako, J. Ye, *Chem. Mater.* **2013**, *25*, 405–411.
- [4] H. Wang, J. Yang, X. Li, H. Zhang, J. Li, L. Guo, *Small* **2012**, *8*, 2802–2806.
- [5] H. Wang, J. Gao, T. Guo, R. Wang, L. Guo, Y. Liu, J. Li, *Chem. Commun.* **2012**, *48*, 275–277.
- [6] a) D. W. Shin, C. A. Bridges, A. Huq, M. P. Paranthaman, A. Manthiram, *Chem. Mater.* **2012**, *24*, 3720–3731; b) S. C. Yan, S. X. Ouyang, J. Gao, M. Yang, J. Y. Feng, X. X. Fan, L. J. Wan, Z. S. Li, J. H. Ye, Y. Zhou, Z. G. Zou, *Angew. Chem. Int. Ed.* **2010**, *49*, 6400–6404; *Angew. Chem.* **2010**, *122*, 6544–6548; c) M. Zhong, Y. Li, I. Yamada, J. J. Delaunay, *Nanoscale* **2012**, *4*, 1509–1514; d) N. Kumagai, L. Ni, H. Irie, *Chem. Commun.* **2011**, *47*, 1884–1886; e) V. B. R. Boppina, R. F. Lobo, *ACS Catal.* **2011**, *1*, 923–928; f) X. Xu, A. K. Azad, J. T. S. Irvine, *Catal. Today* **2013**, *199*, 22–26.
- [7] H. Xue, Z. Li, Z. Ding, L. Wu, X. Wang, X. Fu, *Cryst. Growth Des.* **2008**, *8*, 4511–4516.
- [8] M. M. Maitani, K. Tanaka, D. Mochizuki, Y. Wada, *J. Phys. Chem. Lett.* **2011**, *2*, 2655–2659.
- [9] a) W. Q. Fang, X.-Q. Gong, H. G. Yang, *J. Phys. Chem. Lett.* **2011**, *2*, 725–734; b) T. Tachikawa, N. Wang, S. Yamashita, S.-C. Cui, T. Majima, *Angew. Chem. Int. Ed.* **2010**, *49*, 8593–8597; *Angew. Chem.* **2010**, *122*, 8775–8779.
- [10] S. Chen, D. L. Carroll, *Nano Lett.* **2002**, *2*, 1003–1007.
- [11] Q. Liu, Y. Zhou, Z. Tian, X. Chen, J. Gao, Z. Zou, *J. Mater. Chem.* **2012**, *22*, 2033–2038.
- [12] M. C. Payne, M. P. Teter, D. C. Allan, T. Arias, J. Joannopoulos, *Rev. Mod. Phys.* **1992**, *64*, 1045–1097.
- [13] G. Xi, J. Ye, *Chem. Commun.* **2010**, *46*, 1893–1895.
- [14] X. Zhao, W. Jin, J. Cai, J. Ye, Z. Li, Y. Ma, J. Xie, L. Qi, *Adv. Funct. Mater.* **2011**, *21*, 3554–3563.
- [15] a) M. Hara, M. Komoda, H. Hasei, M. Yashima, S. Ikeda, T. Takata, J. N. Kondo, K. Domen, *J. Phys. Chem. B* **2000**, *104*, 780–785; b) S. Ikeda, T. Takata, M. Komoda, M. Hara, J. N. Kondo, K. Domen, A. Tanaka, H. Hosono, H. Kawazoe, *Phys. Chem. Chem. Phys.* **1999**, *1*, 4485–4491.
- [16] a) N. J. Bell, Y. H. Ng, A. Du, H. Coster, S. C. Smith, R. Amal, *J. Phys. Chem. C* **2011**, *115*, 6004–6009; b) X.-J. Lv, S.-X. Zhou, C. Zhang, H.-X. Chang, Y. Chen, W.-F. Fu, *J. Mater. Chem.* **2012**, *22*, 18542–18549.
- [17] L. Zhang, D. Bahnemann, *ChemSusChem* **2013**, *6*, 283–290.
- [18] J. Yu, B. Wang, *Appl. Catal. B* **2010**, *94*, 295–302.
- [19] A. Hagfeldt, H. Lindström, S. Södergren, S.-E. Lindquist, *J. Electroanal. Chem.* **1995**, *381*, 39–46.
- [20] S. Yan, J. Wang, H. Gao, N. Wang, H. Yu, Z. Li, Y. Zhou, Z. Zou, *Adv. Funct. Mater.* **2013**, *23*, 758–763.
- [21] S. J. Clark, M. D. Segall, C. J. Pickard, P. J. Hasnip, M. I. Probert, K. Refson, M. C. Payne, *Z. Kristallogr.* **2005**, *220*, 567–570.
- [22] W. Kohn, L. J. Sham, *Phys. Rev. A* **1965**, *140*, A1133–A1138.
- [23] a) A. M. Rappe, K. M. Rabe, E. Kaxiras, J. Joannopoulos, *Phys. Rev. B* **1990**, *41*, 1227–1230; b) J. Lin, A. Qteish, M. Payne, V. Heine, *Phys. Rev. B* **1993**, *47*, 4174–4180.
- [24] D. M. Ceperley, B. Alder, *Phys. Rev. Lett.* **1980**, *45*, 566–569.
- [25] H. J. Monkhorst, J. D. Pack, *Phys. Rev. B* **1976**, *13*, 5188–5192.
- [26] L. Bellaiche, D. Vanderbilt, *Phys. Rev. B* **2000**, *61*, 7877–7882.

Received: August 27, 2014

Published online on ■■■■■, 0000



S.-X. Zhou, X.-J. Lv,* C. Zhang, X. Huang, L. Kang, Z.-s. Lin, Y. Chen, W.-F. Fu*



Synthesis of NiGa₂O₄ Octahedron Nanocrystal with Exposed {111} Facets and Enhanced Efficiency of Photocatalytic Water Splitting



Photocatalytic activity: Octahedral NiGa₂O₄ with highly reactive pH-dependent {111} facets have been synthesized through a facile hydrothermal route without using any template or organic

surfactant. The {111} facets of octahedral NiGa₂O₄ display enhanced photocatalytic generation of hydrogen from water splitting and good photocatalytic stability (see figure).